Lithium-Ion Battery Solid Electrolytes Based on Poly(Vinylidene Fluoride) -Metal Thiocyanate Ionic Liquid Blends

João P. Serra[1,2], Arkaitz Fidalgo-Marijuan[3,4], João C. Barbosa[1,2,5], Daniela M. Correia[1,5], Renato Gonçalves[6], José M. Porro[3,7], Senentxu Lanceros-Mendez[3,7*], Carlos M. Costa[1,2,8*]

[1]Physics Centre of Minho and Porto Universities (CF-UM-UP), University of Minho, 4710-057, Portugal

[2]Laboratory of Physics for Materials and Emergent Technologies, LapMET, University of Minho, 4710-057, Portugal

[3]BCMaterials, Basque Center for Materials, Applications and Nanostructures, UPV/EHU Science Park, 48940 Leioa, Spain

[4]Department of Organic and Inorganic Chemistry, University of the Basque Country (UPV/EHU), 48940, Leioa, Spain.

[5]Centre of Chemistry, University of Trás-os-Montes e Alto Douro, 5000-801, Vila Real, Portugal

[6]Centre of Chemistry, University of Minho 4710-057 Braga, Portugal

[7]Ikerbasque, Basque Foundation for Science, 48009 Bilbao, Spain

[8]Institute of Science and Innovation for Bio-Sustainability (IB-S), University of Minho, 4710-057 Braga, Portugal

KEYWORDS: magnetic ionic liquids; poly(vinylidene fluoride); blends; solid polymer electrolyte; solid-state lithium-ion batteries

---

* **Corresponding Authors**

Carlos M. Costa (cmscosta@fisica.uminho.pt)

Senentxu Lanceros-Méndez (senentxu.lanceros@bcmaterials.net)

ABSTRACT: Solid polymer electrolytes (SPEs) are required to improve battery safety through the elimination of the liquid electrolyte solution in current batteries. This work reports on the development of an SPE based on poly(vinylidene fluoride), PVDF, with the magnetic ionic liquid (MIL)1-butyl-3-methylimidazolium cobalt(II) isothiocyanate, $[BMIM]_2[(SCN)_4Co]$, and its battery cycling behavior at room temperature. The addition of MIL in filler contents up to 40wt.%, to the PVDF polymer matrix does not affect the compact morphology of the samples obtained by solvent casting. The polar β-phase of PVDF increases with increasing MIL content, whereas the degree of crystallinity, thermal degradation temperature and mechanical properties of the MIL/PVDF blends decrease with increasing MIL content. The ionic conductivity of the MIL/PVDF blends increases both with temperature and MIL content, showing a highest ionic conductivity of 7×10^{-4} $mS.cm^{-1}$ at room temperature for the MIL/PVDF blend with 40wt. % of MIL. The cathodic half-cells prepared with this blend as SPE show good reversibility and excellent cycling behavior at different C-rates, with a discharge capacity of 80 $mAh.g^{-1}$ at C/10-rate with 99% of coulombic efficiency. The developed magnetic SPE is suitable for the next generation of sustainable lithium-ion batteries with excellent performance at room temperature, which performance can be further tuned by an external magnetic field.

1. INTRODUCTION

Taking into account the constant population growth and the increasing use of resources, two of the most important issues to be tackled by modern society are related to energy and environment [1]. The demand for energy is increasing to satisfy the life quality of the population [2] and much of the world's energy production is based on the use of fossil fuels, their use being responsible for a large production of CO_2 and others greenhouse gases, with the consequent influence in climate change [3].

The energy transition to renewable energy sources represents an important contribution to address energy and environmental concerns. The investment in renewable energy reduces dependence on fossil fuels, thus enabling the production of "cleaner" energy [4-5]. The major problem associated with the majority of renewable energy production is their intermittence and dependence on favourable environmental factors for efficient energy production [6-7]. The absence of wind affects the production of energy from wind turbines, the low sunlight intensity affects the energy production by photovoltaic panels, and low water storage and low flow also affect energy production through hydropower, which can compromise the normal and constant supply of energy [8]. To solve these problems, one of the possible solutions involves the coupling of energy storage systems to energy production systems, in which during the energy production and low energy consumption peaks, the system would allow energy storage for higher energy demanding peaks, avoiding also energy supply failures [9-11].

One of the most widely used energy storage systems are batteries that transform chemical energy into electrical energy and vice versa [12]. Among the most relevant battery types used nowadays are lithium-ion batteries (LIBs) due to their high energy and power density and excellent electrochemical performance, compact size and low weight, low self-discharge and long service life [13-14]. All these characteristics make this type of batteries

one of the most used today in a wide variety of applications, ranging from mobile phones and computers to electric cars) [15]. LIBs consist of two electrodes, the cathode and the anode, separated by a membrane that is soaked in an electrolyte solution [16].

The electrolyte solution is typically composed of lithium salts dissolved in a volatile solution with organic components and is flammable and harmful to the environment, which represents a safety problem for humans and the environment, while also presenting danger of overheating and ignition [17-18]. One of the solutions to overcome this problem is the replacement of the separator/electrolyte with solid polymer electrolytes (SPEs), which are expected to integrate the next generation of batteries [19]. SPEs include dry solid polymer electrolytes (dry-SPEs), single-ion conducting polymer electrolytes and polymer-in-salt systems (rubbery electrolytes), whose current main drawbacks are a low ionic conductivity value and their interfacial interaction with the electrodes [20]. SPEs consist of a polymeric matrix accompanied by one or more fillers. These fillers are essential to provide ionic conductivity to the matrix and to provide mechanical consistency to the SPE [21]. The most used polymers for SPEs development are poly(vinylidene fluoride) (PVDF) [22-23] and its copolymers with hexafluoropropylene (HFP) [24] and poly(ethylene oxide) (PEO) [25], among others. In relation to the fillers, the most commonly used materials are lithium salts such as lithium tetrafluoroborate ($LiBF_4$), lithium perchlorate ($LiClO_4$), lithium hexafluorophosphate ($LiPF_6$) and lithium bis(trifluoromethanesulfonyl)imide (LiTFSI) [26], carbon-based materials (graphene oxide and carbon nanotubes), particulate materials such as, barium titanate ($BaTiO_3$), titanium dioxide (TiO_2) [27] and ionic liquids (ILs) [28], among others. The SPE must present an ionic conductivity of at least > 10^{-5} – 10^{-4} $S.cm^{-1}$ to be used in LIBs.

In particular, ILs are eco-friendly materials with interesting properties for SPE applications, such as low vapor pressure, high ionic conductivity, and high thermal and

chemical stability [29]. Recently, SPEs based on ILs/PVDF and its copolymers have been developed with different ILs: 1-ethyl-3-methylimidazolium bis (trifluoromethylsulfonyl) imide ([EMIM][TFSI]) and 1-butyl-3-methylimidazolium thiocyanate ([BMIM][SCN]). The [BMIM][SCN]/PVDF-HFP SPE with 40 wt.% IL content shows and ionic conductivity of 0.15 $mS.cm^{-1}$ and a discharge capacity of 124 $mAh.g^{-1}$ at C/8-rate [28]. A specific class of ILs are magnetic ionic liquids (MILs) which include paramagnetic compounds (transition metals like Cobalt (Co), Iron (Fe), or Manganese (Mn)) in their structure (cations or anions). The present work proposes the development of blends based on PVDF with MILs for SPE application due to the fact that the magnetic field allows to minimize battery aging, improves the ionic transport through the magnetohydrodynamic force and reduces the growth of the solid electrolyte interface (SEI) [30]. The blends were produced by solvent casting technique with different MIL content. The selected MIL was the 1-butyl-3-methylimidazolium cobalt(II) isothiocyanate, $[BMIM]_2[(SCN)_4Co]$. The morphology, physical–chemical, mechanical, magnetic and electrochemical properties of the MIL/PVDF blends films were evaluated and cathodic C-$LiFePO_4$ half-cells with the blend films were fabricated for the evaluation of the charge-discharge performance of these batteries at room temperature.

2. EXPERIMENTAL DETAILS

2.1.Materials

Poly(vinylidene fluoride) (PVDF, Solef 6010, Mw=352-600 kDa and Solef 5130, Mw=1000-1300 kDa), C-$LiFePO_4$ (LFP), and carbon black (Super P-C45) were acquired from Solvay, Phostech Lithium and Timcal Graphite & Carbon, respectively. The solvents N,N-dimethylformamide (99%) (DMF) and N-methyl-2-pyrrolidone (99%) (NMP) were purchased from Merk and the magnetic ionic liquid (MIL, 1-butyl-3-methylimidazolium cobalt(II) isothiocyanate, $[BMIM]_2[(SCN)_4Co]$, from Iolitec.

2.2.Film preparation

The polymer blends were prepared by a solvent casting process, following the general guidelines presented in [31]. Different amounts of MIL (0 wt.%, 10 wt.%, 20 wt.% and 40 wt.%) were dispersed in DMF under magnetic stirring at 40 ºC. Subsequently, PVDF powder was added to the solution in a polymer to DMF ratio of 15/85wt.% and kept under magnetic stirring until the complete dissolution of the polymer (120 minutes). Finally, the solution was spread on a glass substrate by doctor blade (gap size of 300 μm) followed by solvent evaporation at 210 ºC for 10 minutes in an oven (P-Selecta). Under this processing conditions, neat PVDF typically crystallizes in the non-polar α-phase [31].

Figure 1 shows the schematic representation of the procedure used to prepare the MIL/PVDF blends.

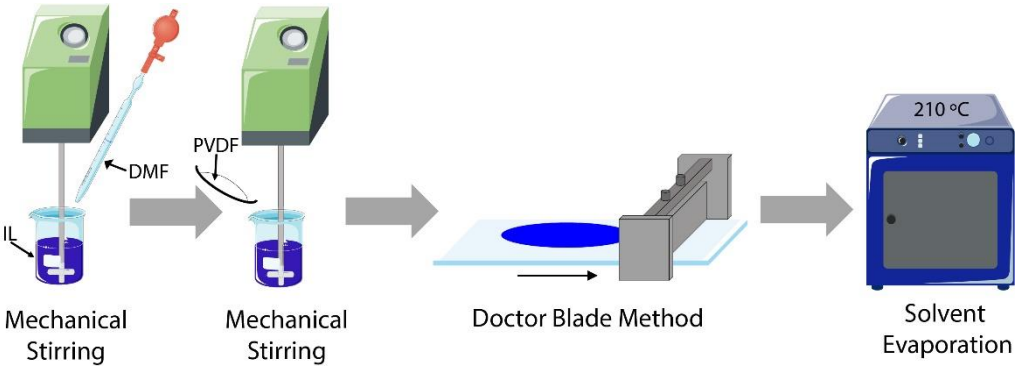

Figure 1. Schematic representation of the procedure used for the preparation of the MIL/PVDF blends.

2.3.Samples characterization

Surface morphology of the MIL/PVDF blends and elemental analysis were evaluated by Scanning Electron Microscopy (SEM) using a Carl Zeiss EVO-40 special edition, set up, equipped with a secondary electron and backscattered electron detector and with an EDS elemental analyzer. The accelerating voltage of the measurements was 20 kV. The blends samples were coated with a thin gold layer for 120 s under $<10^{-4}$ bar pressure and 10 mA current before surface studies by using sputter coater (SC502), Polaron.

The polymer phase was determined by Fourier transform infrared spectroscopy (FTIR) carried out with a Jasco FT/IR-6100 set up in the attenuated total reflection (ATR) mode. Measurements were performed in the spectral range from 4000 to 600 cm^{-1} with a resolution of 4 cm^{-1}. 64 scans were performed in each sample.

For the quantification of the α- and β-phases content in the samples, the specific bands at 766 cm^{-1} and 840 cm^{-1} are used, which correspond to the α- and β-phases of the polymer [32], respectively, together with equation 1 [32]:

$$F(\beta) = \frac{X_\beta}{X_\alpha + X_\beta} = \frac{A_\beta}{(K_\beta/K_\alpha)A_\alpha + A_\beta} \quad (1)$$

where $F(\beta)$ represents the β-phase content, A_α and A_β the absorbances at 766 and 840 cm^{-1}, corresponding to the α- and β-phases of PVDF; K_α and K_β are the absorption coefficients at the respective wave number and X_α and X_β the degree of crystallinity of each phase. The value of K_α is 6.1×10^4 $cm^{-2}.mol^{-1}$ and K_β is 7.7×10^4 $cm^{-2}.mol^{-1}$ [33].

Differential scanning calorimetry (DSC) measurements were carried out with a Perkin-Elmer DSC 6000 instrument under a flowing nitrogen atmosphere between 30 and 200

ºC at a heating rate of 10 ºC.min^{-1}. The samples were measured in 40 µL aluminum pans with perforated lids to allow the release and removal of decomposition products.

The degree of crystallinity of the MIL/PVDF blends is obtained from the DSC scans after equation 2:

$$X_c = \frac{\Delta H_m}{x(\Delta H_{100\%cryst.})_\alpha + y(\Delta H_{100\%cryst.})_\beta} \times 100 \quad (2)$$

where *x* is the weight fraction of the α-phase, *y* is the weight fraction of the β-phase, $(\Delta H_{100\%crystalline})_\alpha$ is the melting enthalpy of pure crystalline α-PVDF and $(\Delta H_{100\%crystalline})_\beta$ is the melting enthalpy of pure crystalline β-PVDF which are reported to be 93.04 J.g^{-1} and 103.4 J.g^{-1}, respectively [34].

Thermogravimetric (TGA) analysis were performed in a TA/SDTA 851e Mettler Toledo apparatus in the range between 25 ºC and 800 ºC at 10 ºC.min^{-1} under a constant air flow of 50 mL.min^{-1}.

The stress-strain mechanical measurements were obtained with a TST350 tensile testing set up from Linkam Scientific Instruments at room temperature and a strain rate of 15 mm.s^{-1}.

The magnetic hysteresis loops of the MIL/PVDF blends were measured with a Micro-Sense EZ7 VSM (Vibrating Sample Magnetometer) by sweeping the magnetic field between -4 kOe and 4 kOe.

Impedance spectroscopy measurements were carried out at open-circuit voltage in an Autolab PGSTAT-12 (Eco Chemie) equipment in the temperature range from 20 to 80 ºC and a frequency range between 500 mHz and 65 kHz, using a constant volume support equipped with gold blocking electrodes located within a Büchi TO 50 oven. The ionic conductivity (σ_i) of the samples was calculated by equation 3:

$$\sigma_i = d/R_b \times A \quad (3)$$

where R_b is the bulk resistance, d is the thickness and A is the area of the sample.

The temperature (T) dependence of the ionic conductivity follows the Arrhenius equation in the measured range:

$$\sigma = \sigma_0 e^{(-E_a/RT)} \quad (4)$$

where E_a is the apparent activation energy, R is the gas constant (8.314 J.mol^{-1}.K^{-1}) and σ_0 is a pre-exponential factor.

The electrochemical stability of the MIL/PVDF blends was evaluated in the two-electrode cell configuration, with a gold microelectrode as working electrode and a lithium disk (Aldrich, 99.9 %; 9 mm diameter, 0.75 mm thick) as counter electrode, through cyclic voltammetry within a dry argon-filled glove-box using an Autolab PGSTAT-12 (Eco Chemie) equipment at a scan rate of 100 mVs^{-1}.

2.4.Cathode electrode and battery preparation. Battery cycling evaluation

The cathode was prepared using 80 wt.% C-LiFePO$_4$, 10 wt.% carbon black and 10 wt.% PVDF 5130 in 2.25 mL of NMP for 1g of solid material. More details on electrode preparation are reported in [35]. The resulting slurry was then casted on aluminum foil by doctor-blade technique and dried at 80 ºC for 2 h. The active mass loading was ~ 1.2 mg.cm^{-2}.

Swagelok type Li/C-LiFePO$_4$ half-cells were assembled in a home-made argon-filled glove box and the MIL/PVDF blends as SPE (10 mm diameter). Metallic lithium (8 mm diameter) was used as anode and the C-LiFePO$_4$ based electrode as cathode (8 mm diameter). Charge-discharge tests were obtained at room temperature in a voltage range of 2.5 V to 4.2 V at current rates from C/10 to C/5 (C = 170 mAh.g^{-1}) using a Landt CT2001A Instrument.

The electrical properties of the Li/C-$LiFePO_4$ half-cells were measured by electrochemical impedance spectroscopy (EIS) before and after cycling with an Autolab PGSTAT12 instrument, in the frequency range from 10 mHz to 1 MHz with an AC voltage amplitude of 10 mV.

3. RESULTS AND DISCUSSION

3.1. Morphological and physicochemical characterization

3.1.1. MIL/PVDF blends morphology and polymer phase

The effect of MIL content on the PVDF blends morphology is shown in Figure 2 through representative surface and cross-section SEM images. Neat PVDF (Figure 2a and b) shows the typical compact morphology of PVDF crystallized after solvent evaporation above the melting temperature. Solvent evaporation at T = 210°C improves polymer chain diffusion to occupy the free space left by the solvent [36].

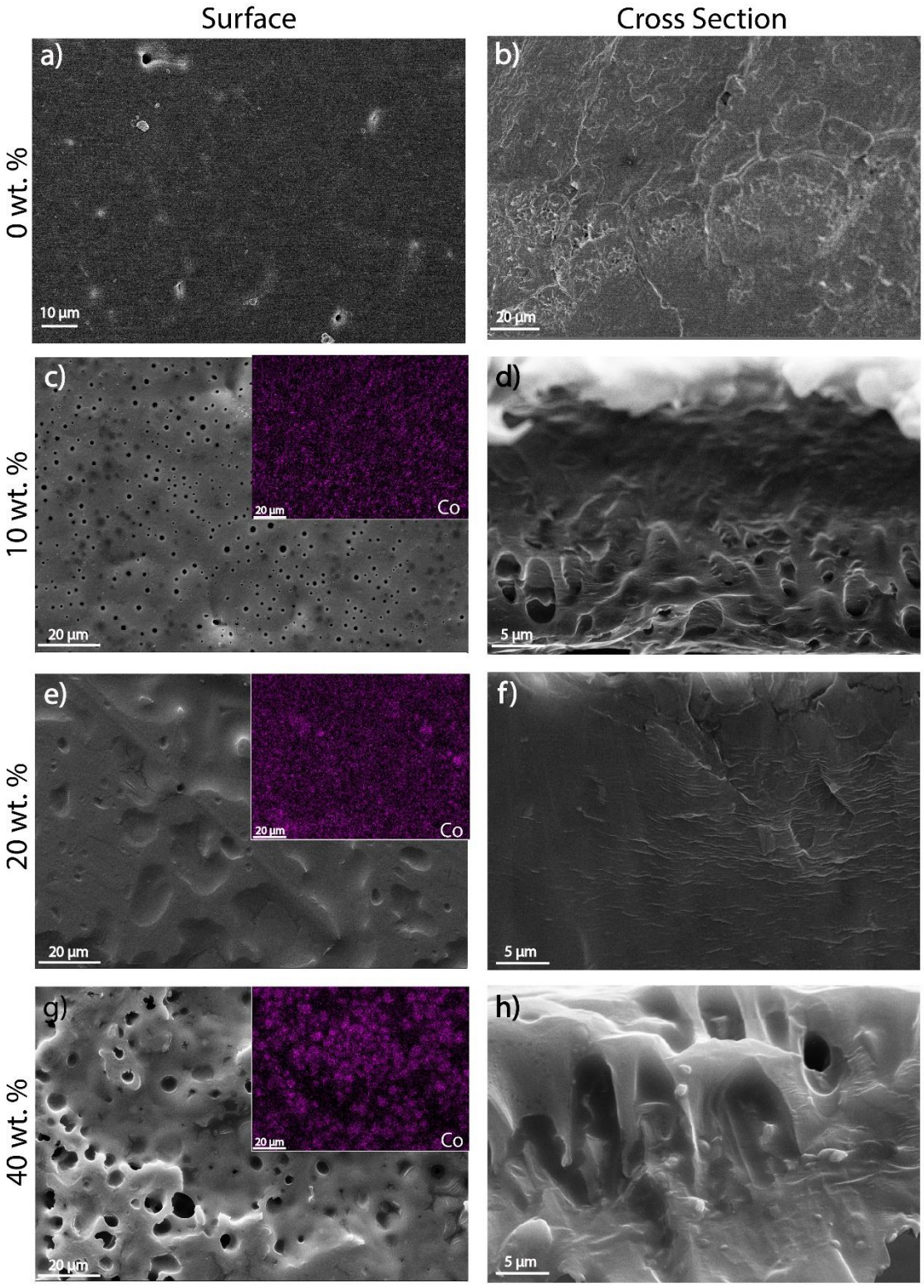

Figure 2. Surface and cross section SEM images of the MIL/PVDF blends with different IL contents a-b) 0 wt.%, c-d) 10 wt.%, e-f) 20 wt.% and g-h) 40 wt.%. Insets: EDS images for the cobalt element in the corresponding MIL/PVDF blends.

The incorporation of different MIL contents (10, 20 and 40 wt.%) into the PVDF matrix, induces changes in the blends surface with respect to the pristine polymer as can be observed in Figures 2c-h. MIL/PVDF blends with 10 and 20 wt.% filler content present a small surface roughness with well-defined spherulitic structure, while for the blend with 40 wt.% the presence of small pores on its surface is evidenced (Figure 2g). The obtained surface microstructure is attributed to the electrostatic interaction that occurs between the IL and the polar DMF solvent, leading to some IL migration to the surface during the solvent evaporation process.

The cross-section of the samples shows that, independently of the filler content, all samples present a compact morphology (Figure 2d-f-h), such as neat PVDF polymer.

Further, energy dispersive spectroscopy (EDS) measurements show the uniform distribution of cobalt (purple colour), a constituent element of the MILs, independently of the filler content (insets of Figure 2c, 2e and 2g).

Increasing filler content leads to the formation of small MIL agglomerates, being higher for the MIL/PVDF blends with 40 wt.% filler content. These agglomerates are nevertheless well distributed across the sample, as demonstrated by the EDS images shown in Figure 2g.

The determination (Figure 3a) and quantification (Figure 3b) of the crystalline phase of PVDF in the different samples was evaluated by FTIR-ATR measurements.

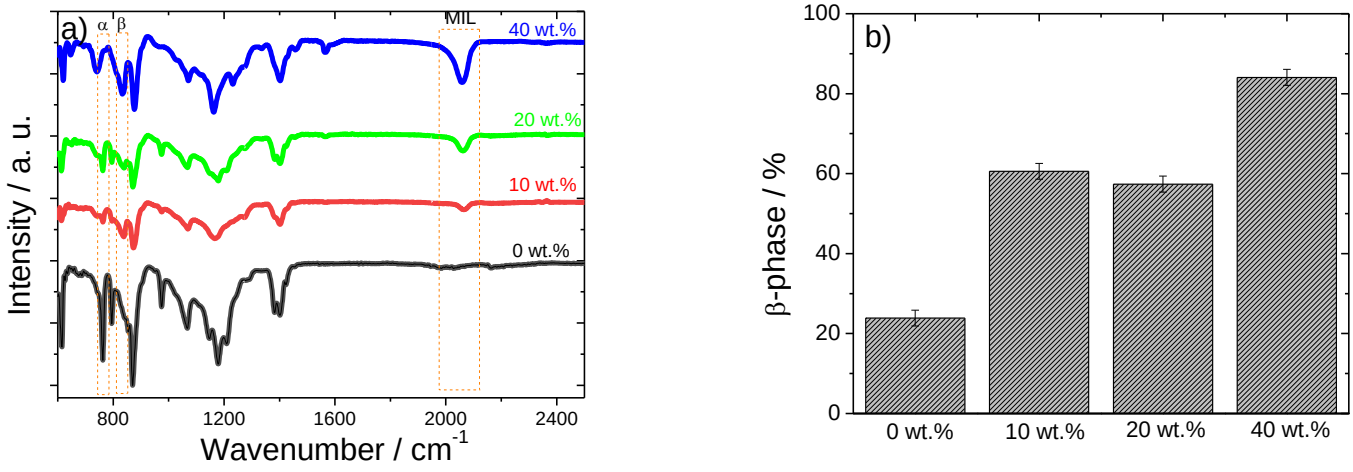

Figure 3. a) FTIR spectra and b) β-phase content for the PVDF blends samples comprising different MIL contents.

The main characteristic PVDF bands of the α- and β-phases (766 and 840 cm^{-1}, respectively) are identified in Figure 3a). Regardless of the amount of MIL present in the PVDF polymer, the polymer crystallizes in a mixture of both crystalline phases [32], but the band corresponding to the β-phase (840 cm^{-1}) increases with increasing MIL content. Other absorption bands characteristics of α-phase (796, 855 and 976 cm^{-1}) and β-phase (1232 cm^{-1}) are also identified in the spectra of Figure 3a). Furthermore, a vibration band at 2050 cm^{-1} that corresponds to the thiocyanate anion related to the C-N stretching [37] is also detected in the blends, which increases with increasing MIL content within the polymer matrix.

The polar β-phase content (%) for the different samples was evaluated by equation 1 and the results are shown in Figure 3b. It is observed that the introduction of MIL into the polymer matrix leads to a strong increase of the fraction of the polymer crystallized in the polar β-phase, leading to electroactive phase contents above 80% for the sample with 40 wt.% MIL content. The preferential crystallization of the polymer in the β-phase in the presence of the MIL is attributed to the ion-dipole interactions, leading the PVDF chains to crystallize in a preferential *all-trans* conformation [38].

3.1.2. Thermal, mechanical and magnetic analysis

The effect of MIL content in the thermal properties of the samples was evaluated by DSC and TGA thermograms (Figure 4).

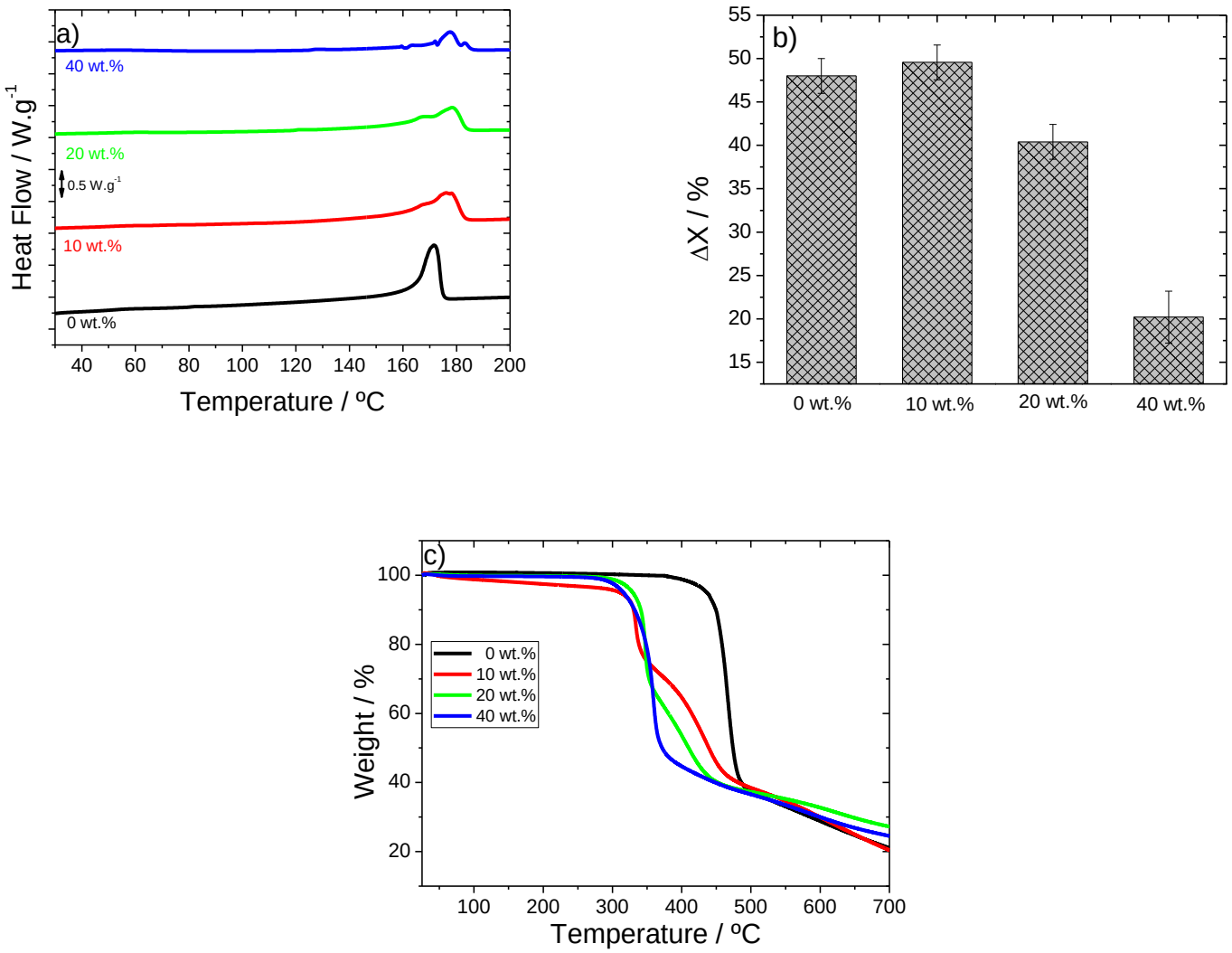

Figure 4. DSC thermograms of PVDF and MIL/PVDF blends incorporating different IL contents (10, 20 and 40 wt.%) from: a) 30ºC to 200ºC, b) degree of crystallinity and c) TGA thermograms of the different samples.

Figure 4a) shows the DSC thermograms measured between 30 and 200 °C to evaluate the influence of the IL content on the melting behaviour of PVDF. Neat PVDF is characterized by a single melting peak at 171 ºC [32]. The inclusion of the MIL in the MIL/PVDF blends leads to a double endothermic peak that becomes more evident with

increasing IL content, which indicates the presence of the two crystal structures (α- and β-phase), as previously observed in the FTIR-ATR spectra (Figure 3) [39]. The endothermic peak at 177 ºC shows that the PVDF melting temperature is shifted to higher temperatures with increasing MIL content, which is attributed to the larger β-phase content [32]. The degree of crystallinity of the MIL/PVDF blends was evaluated by equation 2 and the results are shown in Figure 4b, showing that the degree of crystallinity (ΔX) decreases with the incorporation and the increase of the MIL content except for 10wt.% filler content sample, in which of MIL that acts a nucleation agent. These facts are indicative of the strong interactions between the MIL with the PVDF chains, that hinder polymer crystallization for the larger filler contents, whereas for smaller filler contents act as nucleation zones for polymer crystallization [38, 40].

Figure 4c) shows the TGA thermograms of the MIL/PVDF blends. Neat PVDF shows a single maximum degradation step around 450 ºC corresponding to the scission of carbon-hydrogen (C-H) and carbon-fluorine (C-F) bonds [41]. For MIL/PVDF blends, two degradation steps are detected at ~ 300 ºC and 400 ºC, respectively, except for the blend with 40wt.% MIL content, attributed to the degradation temperature of the MIL [37] and the PVDF polymer [42], respectively. It is interesting to observe that the thermal degradation of PVDF in the MIL/PVDF blends has a strong shift to lower temperatures, slightly dependent on the MIL content, being the strong ion-dipole interactions between MIL and polymer responsible to this effect [43].

Figure 5a) shows the stress-strain curves of neat PVDF and MIL/PVDF blends. All samples show the typical thermoplastic mechanical behaviour of PVDF, characterized by an elastic and a plastic regions separated by yielding [44]. The Young modulus was determined in the elastic region by the tangent method at 3% of the elongation being obtained a maximum and minimum E´ value of 880 MPa and 133 MPa for PVDF and the

MIL/PVDF blends with 40 wt.%, respectively, according to the insert in the Figure 5a). The obtained E´ values indicates that incorporation of the MIL into the PVDF matrix induces a plasticizing behaviour within the blend sample.

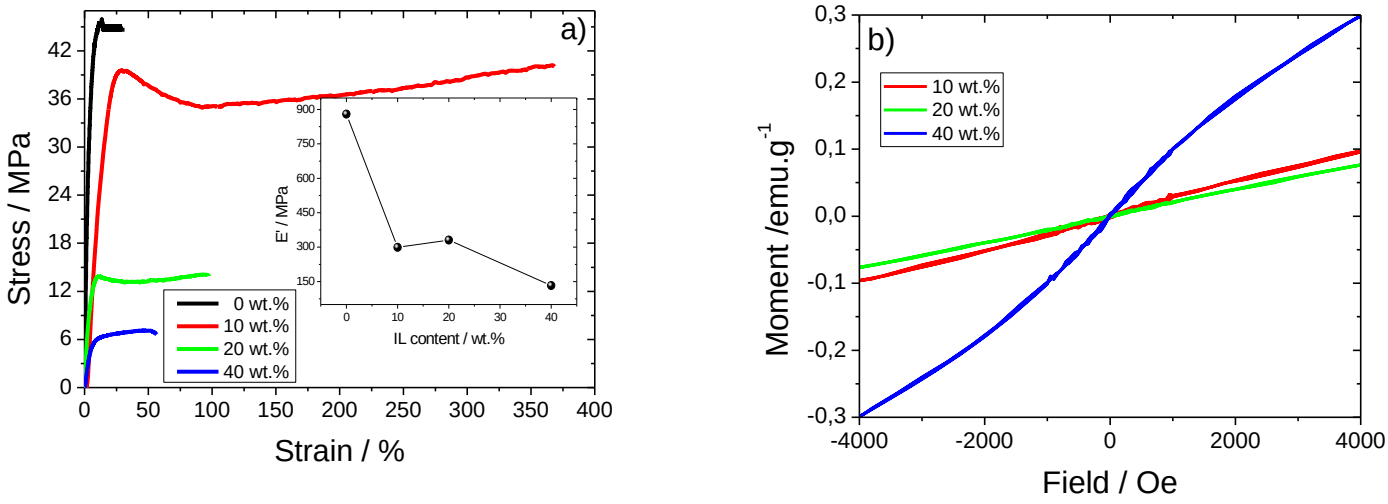

Figure 5. a) Stress-strain curves (insert Young modulus as a function of MIL content) and b) room-temperature magnetic hysteresis loops for PVDF and MIL/PVDF blends with 10, 20 and 40 wt.% of MIL.

Furthermore, it is observed that Young modulus and yield stress decreases with increasing MIL content in the PVDF polymer due to the decreased degree of crystallinity and the plasticizing effect of the MIL. Moreover, it is observed that MIL addition improves the elongation at break of the samples, compared to neat PVDF. This behaviour depends on the MIL content and is higher when 10 wt.% of MIL is added to the PVDF with a maximum strain percentage around 375%.

The magnetic properties of the MIL/PVDF blends were evaluated by vibrating sample magnetometry measurements at room temperature. Figure 5b shows the magnetization as a function of the applied magnetic field for each of the blends studied here. While a linear paramagnetic correlation between the magnetization and the magnetic field is observed for the lower content (10 and 20 wt.% MIL), the 40 wt.% MIL blend starts to show an

incipient ferromagnetic behaviour, while the magnetization of the blends increases with the wt.% MIL. This is a consequence of the higher Co content on the higher wt.% MIL blend.

3.3. Ionic conductivity and electrochemical stability window

The electrochemical performance of the MIL/PVDF blends was evaluated by impedance spectroscopy.

Figure 6a) shows the Nyquist plots of the 40 wt.% MIL/PVDF blends at three different temperatures (30, 60 and 90 ^{o}C) which present two well defined regions: a semicircle located in the high frequency range that corresponds to a charge transfer process and a straight line at lower frequencies that describes the charge diffusion process [45].

The impedance values depend on the temperature and the semicircle related to the charge transfer process decreases with increasing temperature. This is related to the fact that temperature increase leads, on one hand, to faster internal modes in the polymer chains, the bond rotations supporting intra-chain ion movements [46]. On the other hand, increasing temperature leads to improved thermally activated dynamics of the ions of the MIL. This behavior is also representative of the ones of the MIL/PVDF blends with 10 and 20 wt.% MIL content.

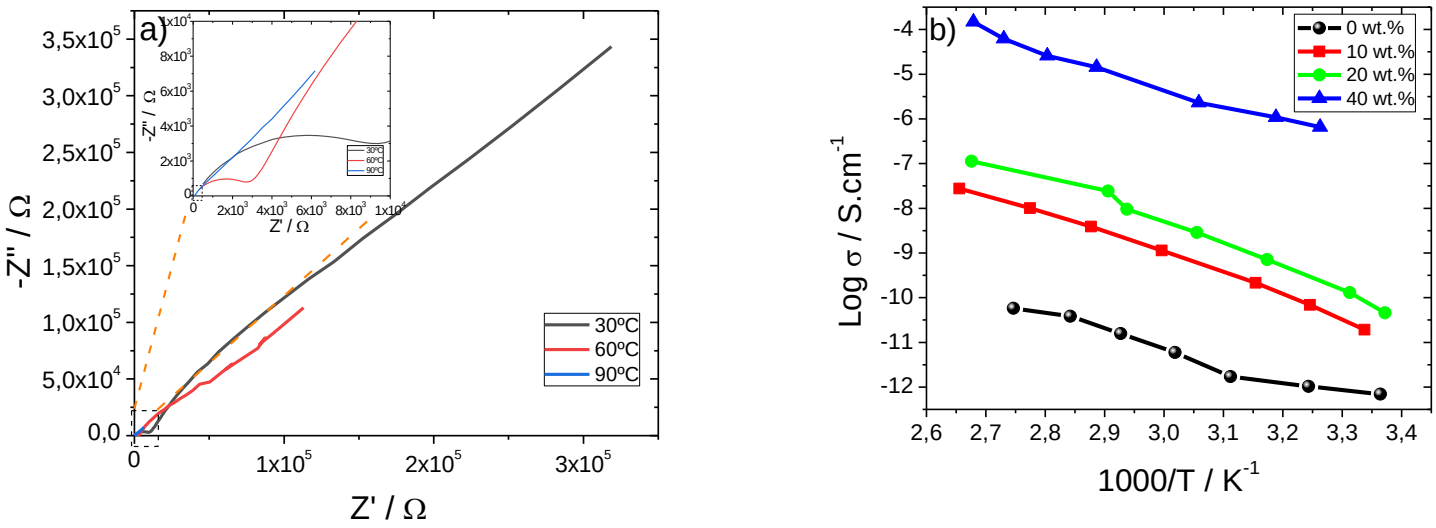

Figure 6. a) Nyquist plots of the 40 wt.% MIL/PVDF blends at different temperatures (30, 60 and 90 ºC) and b) Arrhenius plots for the ionic conductivities of the MIL/PVDF blends with different MIL content.

The ionic conductivity was evaluated from the Nyquist plot presented in Figure 6a, using equation 3, where R_b is obtained from the intercept of the imaginary impedance Z´´ to the real impedance Z´. Figure 6b shows the ionic conductivity variation as a function of temperature for the different MIL/PVDF blends. The ionic conductivity value (σi) and the apparent activation energy (Ea) were calculated by fittings to the Arrhenius equation [47] and the results for the different samples are shown in Table 1. The ionic conductivity value at room temperature for neat PVDF is 7×10^{-10} mS.cm^{-1}.

Table 1. Ionic conductivity (σ_i) and the apparent activation energy (E_a) for the MIL/PVDF blends.

IL/PVDF	**% wt. IL**	**σ_i/ mS.cm^{-1} (25 ºC) (±3%)**	**Ea / kJ.mol^{-1} (±3%)**
$[BMIM]_2[(SCN)_4Co]$	0wt.%	7×10^{-10}	181
	10wt.%	1.9×10^{-8}	38
	20wt.%	4.6×10^{-8}	41

	40wt.%	7×10^{-4}	32

Figure 6b shows that, regardless of the temperature, the ionic conductivity increases with MIL content increase in the PVDF matrix due to the increase of number of charge carriers, anions and cations of the MIL, within the polymer matrix. The highest ionic conductivity value at room temperature is obtained for 40 wt.% MIL/PVDF blends with a value of 7×10^{-4} mS.cm^{-1}. In addition, Table 2 shows the ionic conductivity for the 40 wt.% MIL/PVDF blend compared to the current literature on SPEs based on ILs. The present MIL shows an ionic conductivity up to 2 orders of magnitude lower than the best ones in the literature, though enough for battery applications and with the characteristic of presenting magnetic response, which can be suitable for LIBs, as it has been reported that the application of a magnetic field reduces the aging effect, inhibits SEI growth and lithium plating, and also homogenizes ionic transport through the magnetohydrodynamic force [30].

Table 2. Ionic conductivity value for different SPEs with ILs.

Polymer	**Components**	**σ_i(mS.cm^{-1}) at 25 °C**	**Ref**
PI	[Bmim][TFSI], LiTFSI	1.7×10^{-2}	[48]
PEO, PVDF	LiTFSI, POSS-IL	80×10^{-2}	[49]
PEO, PVDF-HFP, PC	LiTFSI, POSS-IL	39×10^{-2}	[50]
PVDF-HFP	[BMIM][SCN]	15×10^{-2}	[51]
PEO	LiDFOB-[EMIM][TFSI]	7×10^{-3}	[52]
PVDF	$[BMIM]_2[(SCN)4Co]$	7×10^{-4}	This work

Figure 7 shows the electrochemical stability of the MIL/PVDF blends at room temperature and at 100 mV.s^{-1}.

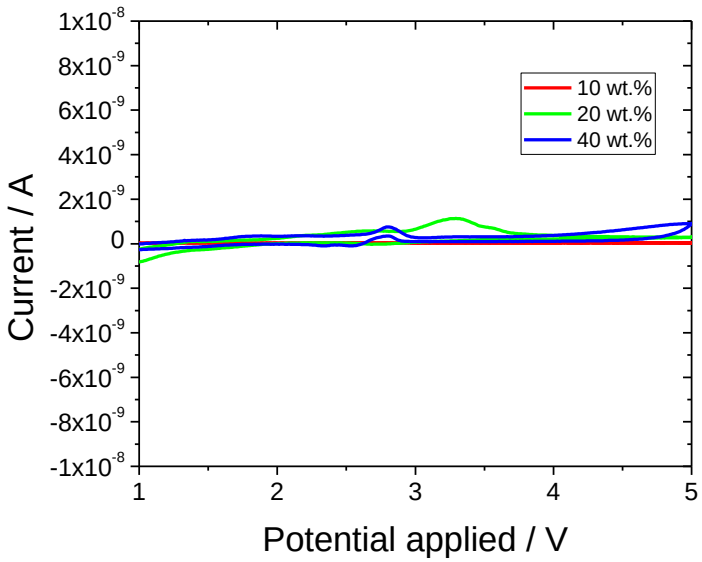

Figure 7. Cyclic voltammogram of the different blends at room temperature and 100 $mV.s^{-1}$.

Regardless of the MIL/PVDF blends, all samples show good electrochemical stability in the 1 to 5 V range, considering the current in order of nA. Furthermore, a small anodic peak is observed in the different blends, attributed to irreversible processes within the MIL-polymer blend, which does not affect the cycling behaviour considering its value in the order of nA. Finally, it is observed that the cyclic voltammgram presents a reversible behavior for the SPE, being suitable for battery applications.

3.4. Battery performance

Taking into account that the highest ionic conductivity was obtained for the sample with 40 wt.% MIL, the cycling performance was evaluated for this sample in cathodic half-cells with C-LFP. Cycling was carried out at room temperature at C/10, C/8 and C/5-rates, in the potential window between 2.5 V and 4.2 V that corresponds to voltage range of the LFP structure without causing any damage to it. Figure 8a shows the typical charge-discharge profile for the 1st, 20th, 30th, 40th and 50th cycles at C/8-rate. This profile is typical of the active material C-$LiFePO_4$ cathode [53] and the charge and discharge values

decrease after the 50 cycle due to the solid electrolyte interface (SEI) layer formation during cycling [54], demonstrating nevertheless a good reversibility process.

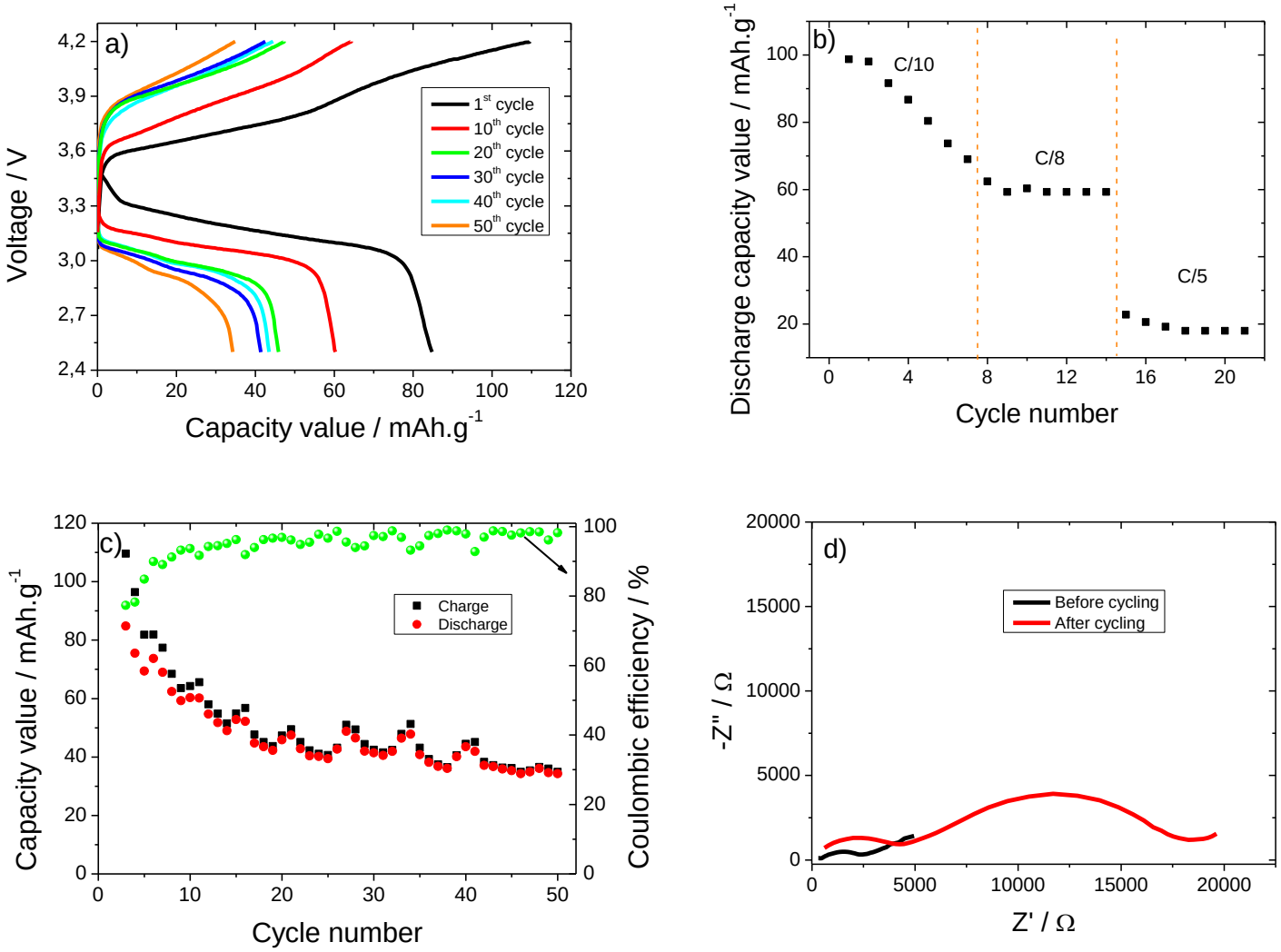

Figure 8. a) 1st, 20th, 30th, 40th and 50th charge and discharge room temperature cycles at C/8 rate, b) rate performance as a function of the cycle number, c) cycling performance at C/8 rate and d) impedance spectra before and after cycling for the 40 wt.% MIL/PVDF SPE based cathodic half-cells.

Figure 8b) shows the rate performance at three different C-rates for 7 cycles at each rate and room temperature. For each rate in the 7th cycle, the discharge capacity values are 80 mAh.g^{-1}, 61 mAh.g^{-1} and 17 mAh.g^{-1} at the C rates of C/10, C/8 and C/5, respectively. For the C/8-rate, it is observed that the discharge capacity value decreases as a function

of the cycle number due to the SEI formation. Furthermore, for other C-rates, the discharge capacity value is almost constant. Also, it is detected that when the C-rate increases, the discharge capacity value decreases due to the polarization effect and the interfacial reaction resistance within the electrode [55].

Figure 8c shows the charge/discharge capacity values at the C/8-rate for 50 cycles. The discharge capacity values are 72 $mAh.g^{-1}$ and 30 $mAh.g^{-1}$, respectively, in the 1^{st} and 50^{th} cycle and the coulombic efficiency is about 99%. It is observed that the electrochemical behaviour decreases up to 15 cycles due to the SEI layer formation. It is to notice that the observed charge/discharge capacity value wave-like fluctuations are not dependent on the SPE, but on the daily temperature fluctuations of the laboratory. Further, excellent coulombic efficiency is observed after the 50 cycles, which indicates good reversibility in the process.

Figure 8d shows the EIS spectra for the batteries before and after cycling.

For both spectra, the Nyquist plot is composed by two semicircles at high and medium frequencies, that represent the contact film resistance and resistance contributions from the charge-transfer reaction resistance, and a straight line at low frequency region that represents the Li^+ diffusion process characterized by Warburg element [56].

It is observed that the overall resistance (ohmic resistance, contact film resistance and charge-transfer reaction resistance) before and after cycling are 2450 Ω and 18285 Ω, respectively. This increase is due to the formation of a SEI layer during cycling [54].

It is to notice that most current literature on polymer matrix SPE, shows battery performance at temperatures above 50 ºC [57-59], which limits its applicability, whereas in the present case, the battery performance is evaluated and presented at room temperature.

In summary, considering the battery performance at room temperature for this SPE with IL, this work demonstrates a step forward in the development of SPEs for the next

generation of lithium-ion batteries. The use of MILs in LIBs is a promising approach due to its possibility to reduce the aging effects and achieve higher battery performance resulting from lower SEI growth and ion transport homogenization, when a magnetic field is applied [30].

4. CONCLUSIONS

Solid polymer electrolytes, SPEs, based on PVDF and the $[BMIM]_2[(SCN)_4Co]$ magnetic ionic liquid, MIL, have been prepared by solvent casting at 210 ºC and the effect of MIL content on morphology, physical, thermal, mechanical, magnetic and electrochemical properties has been evaluated.

MIL/PVDF blends show a compact morphology independently of the filler content and the β-phase content. Their thermal and mechanical properties are influenced by the MIL content in the PVDF matrix. The β-phase content increases with increasing MIL content due to the electrostatic interactions between the MIL and the polymer chains. The degree of crystallinity of the blends decreases from 48% to 20% with increasing MIL content. Similarly, the thermal stability of the samples decreases upon higher MIL incorporation rates. Independently of the MIL content, its incorporation into the PVDF matrix induces a plasticizing behavior, reducing the Young modulus from 880 MPa to 133 MPa. In addition, a crossover from a paramagnetic to an incipient ferromagnetic behavior in the blends is observed as the MIL content is increases.

The ionic conductivity of the samples depends on the MIL content and the temperature. The highest ionic conductivity at room temperature is 7×10^{-4} $mS.cm^{-1}$ for the MIL/PVDF blends with 40 wt.%. Also, these blends show excellent electrochemical stability in the potential window up to 5V.

Battery performance for the MIL/PVDF blends with 40wt.% filler content in cathodic half-cells at room temperature shows good reversibility and the discharge capacity values are 80 $mAh.g^{-1}$, 61 $mAh.g^{-1}$ and 17 $mAh.g^{-1}$ at the C rates of C/10, C/8 and C/5, respectively, demonstrating excellent cycling behavior at room temperature and 99% of coulombic efficiency. Furthermore, after 50 cycles at the C/8-rate, the cycle behavior is nearly constant, demonstrating the suitability of this SPE for the next generation of LIBs able to take advantage of the application of magnetic fields to improve battery performance by reducing aging and SEI growth as well as to improve ion transport through the magnetohydrodynamic force.

AUTHOR INFORMATION

Corresponding Authors

cmscosta@fisica.uminho.pt (Carlos M. Costa),

senentxu.lanceros@bcmaterials.net (Senentxu Lanceros-Méndez)

Author Contributions

The manuscript was written through contributions of all authors. All authors have given approval to the final version of the manuscript

Notes

The authors declare no competing financial interest.

ACKNOWLEDGEMENTS

The authors thank the Fundação para a Ciência e Tecnologia (FCT) for financial support under the framework of Strategic Funding UIDB/04650/2020, UID/FIS/04650/2020, UID/EEA/04436/2020, and UID/QUI/0686/2020 and under projects POCI-01-0145-

FEDER-028157, MIT-EXPL/TDI/0033/2021, POCI-01-0247-FEDER-046985 and PTDC/FIS-MAC/ 28157/2017 funded by national funds through FCT and by the ERDF through the COMPETE2020—Programa Operacional Competitividade e Internacionalização (POCI). The authors also thank the FCT for financial support under Grants 2021.08158.BD (J.P.S), SFRH/BD/140842/2018 (J.C.B.), SFRH/BPD/121526/2016 (D.M.C) and FCT investigator contracts CEECIND/00833/2017 (RG) and 2020.04028.CEECIND (C.M.C.). Financial support from the Basque Government Industry Department under the ELKARTEK program is acknowledged. The authors thank for technical and human support provided by SGIker (UPV/EHU/ ERDF, EU).

REFERENCES

1. Liu, J.; Hull, V.; Godfray, H. C. J.; Tilman, D.; Gleick, P.; Hoff, H.; Pahl-Wostl, C.; Xu, Z.; Chung, M. G.; Sun, J. Nexus Approaches to Global Sustainable Development. *Nature Sustainability* **2018,** *1*, 466-476.

2. Nadimi, R.; Tokimatsu, K. Energy Use Analysis in the Presence of Quality of Life, Poverty, Health, and Carbon Dioxide Emissions. *Energy* **2018,** *153*, 671-684.

3. Lin, B.; Jia, Z. Economic, Energy and Environmental Impact of Coal-to-Electricity Policy in China: A Dynamic Recursive Cge Study. *Science of the Total Environment* **2020,** *698*, 134241.

4. Davidson, D. J. Exnovating for a Renewable Energy Transition. *Nature Energy* **2019,** *4*, 254-256.

5. Vakulchuk, R.; Overland, I.; Scholten, D. Renewable Energy and Geopolitics: A Review. *Renewable and Sustainable Energy Reviews* **2020,** *122*, 109547.

6. Das, P.; Mathur, J.; Bhakar, R.; Kanudia, A. Implications of Short-Term Renewable Energy Resource Intermittency in Long-Term Power System Planning. *Energy strategy reviews* **2018,** *22*, 1-15.

7. Baum, Z.; Palatnik, R. R.; Ayalon, O.; Elmakis, D.; Frant, S. Harnessing Households to Mitigate Renewables Intermittency in the Smart Grid. *Renewable Energy* **2019,** *132*, 1216-1229.

8. Jiang, B.; Farid, A. M.; Youcef-Toumi, K. Demand Side Management in a Day-Ahead Wholesale Market: A Comparison of Industrial & Social Welfare Approaches. *Applied Energy* **2015,** *156*, 642-654.

9. Geem, Z. W.; Yoon, Y. Harmony Search Optimization of Renewable Energy Charging with Energy Storage System. *International Journal of Electrical Power & Energy Systems* **2017,** *86*, 120-126.

10. Lee, S.-J.; Yoon, Y. Electricity Cost Optimization in Energy Storage Systems by Combining a Genetic Algorithm with Dynamic Programming. *Mathematics* **2020,** *8*, 1526.

11. Abdalla, A. N.; Nazir, M. S.; Tao, H.; Cao, S.; Ji, R.; Jiang, M.; Yao, L. Integration of Energy Storage System and Renewable Energy Sources Based on Artificial Intelligence: An Overview. *Journal of Energy Storage* **2021,** *40*, 102811.

12. Schmidt-Rohr, K. How Batteries Store and Release Energy: Explaining Basic Electrochemistry. *Journal of Chemical Education* **2018,** *95*, 1801-1810.

13. Roy, J. J.; Cao, B.; Madhavi, S. A Review on the Recycling of Spent Lithium-Ion Batteries (Libs) by the Bioleaching Approach. *Chemosphere* **2021,** 130944.

14. Christensen, P. A.; Anderson, P. A.; Harper, G. D.; Lambert, S. M.; Mrozik, W.; Rajaeifar, M. A.; Wise, M. S.; Heidrich, O. Risk Management over the Life Cycle of

Lithium-Ion Batteries in Electric Vehicles. *Renewable and Sustainable Energy Reviews* **2021,** *148*, 111240.

15. Pillot, C. In *The Rechargeable Battery Market and Main Trends 2018-2030*, 36th Annual International Battery Seminar & Exhibit. Avicenne Energy, **2019**.

16. Miranda, D.; Gören, A.; Costa, C.; Silva, M. M.; Almeida, A.; Lanceros-Méndez, S. Theoretical Simulation of the Optimal Relation between Active Material, Binder and Conductive Additive for Lithium-Ion Battery Cathodes. *Energy* **2019,** *172*, 68-78.

17. Gonçalves, R.; Miranda, D.; Almeida, A.; Silva, M. M.; Meseguer-Dueñas, J. M.; Ribelles, J. G.; Lanceros-Méndez, S.; Costa, C. Solid Polymer Electrolytes Based on Lithium Bis (Trifluoromethanesulfonyl) Imide/Poly (Vinylidene Fluoride-Co-Hexafluoropropylene) for Safer Rechargeable Lithium-Ion Batteries. *Sustainable Materials and Technologies* **2019,** *21*, e00104.

18. Liu, Y.; Liu, Q.; Xin, L.; Liu, Y.; Yang, F.; Stach, E. A.; Xie, J. Making Li-Metal Electrodes Rechargeable by Controlling the Dendrite Growth Direction. *Nature Energy* **2017,** *2*, 1-10.

19. Barbosa, J. C.; Gonçalves, R.; Costa, C. M.; de Zea Bermudez, V.; Fidalgo-Marijuan, A.; Zhang, Q.; Lanceros-Méndez, S. Metal–Organic Frameworks and Zeolite Materials as Active Fillers for Lithium-Ion Battery Solid Polymer Electrolytes. *Materials Advances* **2021,** *2*, 3790-3805.

20. Long, L.; Wang, S.; Xiao, M.; Meng, Y. Polymer Electrolytes for Lithium Polymer Batteries. *Journal of Materials Chemistry A* **2016,** *4*, 10038-10069.

21. Barbosa, J. C.; Dias, J. P.; Lanceros-Méndez, S.; Costa, C. M. Recent Advances in Poly (Vinylidene Fluoride) and Its Copolymers for Lithium-Ion Battery Separators. *Membranes* **2018,** *8*, 45.

22. Wu, Y.; Li, Y.; Wang, Y.; Liu, Q.; Chen, Q.; Chen, M. Advances and Prospects of Pvdf Based Polymer Electrolytes. *Journal of Energy Chemistry* **2021,** *64*, 62-84.

23. Costa, C. M. S.; Cardoso, V. F.; Brito-Pereira, R.; Martins, P. M. A.; Correia, D. M. S.; Correia, V.; Ribeiro, C. M. O.; Martins, P. L. A.; Lanceros-Méndez, S. Electroactive Poly (Vinylidene Fluoride) Based Materials: Recent Progress, Challenges and Opportunities. **2020,** Elsevier.

24. Lestariningsih, T.; Sabrina, Q.; Ratri, C.; Nuroniah, I. In *Structure, Thermal and Electrical Properties of Pvdf-Hfp/Libob Solid Polymer Electrolyte*, Journal of Physics: Conference Series, IOP Publishing: **2019**; p 012026.

25. Putri, R. M.; Floweri, O.; Mayangsari, T. R.; Aimon, A. H.; Iskandar, F. Preliminary Study of Electrochemical Properties of Polyethylene Oxide (Peo) and Polyvinyl Alcohol (Pva) Composites as Material for Solid Polymer Electrolyte. *Materials Today: Proceedings* **2021,** *44*, 3375-3377.

26. Banitaba, S. N.; Semnani, D.; Fakhrali, A.; Ebadi, S. V.; Heydari-Soureshjani, E.; Rezaei, B.; Ensafi, A. A. Electrospun Peo Nanofibrous Membrane Enable by Licl, Liclo 4, and Litfsi Salts: A Versatile Solvent-Free Electrolyte for Lithium-Ion Battery Application. *Ionics* **2020,** *26*, 3249-3260.

27. Chen, H.; Zheng, M.; Qian, S.; Ling, H. Y.; Wu, Z.; Liu, X.; Yan, C.; Zhang, S. Functional Additives for Solid Polymer Electrolytes in Flexible and High-Energy-Density Solid-State Lithium-Ion Batteries. *Carbon Energy* **2021,** *3*, 929-956.

28. Serra, J.; Pinto, R.; Barbosa, J.; Correia, D.; Gonçalves, R.; Silva, M.; Lanceros-Mendez, S.; Costa, C. Ionic Liquid Based Fluoropolymer Solid Electrolytes for Lithium-Ion Batteries. *Sustainable Materials and Technologies* **2020,** *25*, e00176.

29. Correia, D. M.; Fernandes, L. C.; Martins, P. M.; García-Astrain, C.; Costa, C. M.; Reguera, J.; Lanceros-Méndez, S. Ionic Liquid–Polymer Composites: A New

Platform for Multifunctional Applications. *Advanced Functional Materials* **2020,** *30*, 1909736.

30. Costa, C. M.; Merazzo, K. J.; Gonçalves, R.; Amos, C.; Lanceros-Méndez, S. Magnetically Active Lithium-Ion Batteries Towards Battery Performance Improvement. *iScience* **2021,** *24*, 102691.

31. Ribeiro, C.; Costa, C. M.; Correia, D. M.; Nunes-Pereira, J.; Oliveira, J.; Martins, P.; Gonçalves, R.; Cardoso, V. F.; Lanceros-Méndez, S. Electroactive Poly(Vinylidene Fluoride)-Based Structures for Advanced Applications. *Nature Protocols* **2018,** *13*, 681-704.

32. Martins, P.; Lopes, A. C.; Lanceros-Mendez, S. Electroactive Phases of Poly(Vinylidene Fluoride): Determination, Processing and Applications. *Progress in Polymer Science* **2014,** *39*, 683-706.

33. Salimi, A.; Yousefi, A. A. Analysis Method: Ftir Studies of B-Phase Crystal Formation in Stretched Pvdf Films. *Polymer Testing* **2003,** *22*, 699-704.

34. Lovinger, A. J. Developments in Crystalline Polymers. Basset, D. C., Ed. Elsevier: London, **1982**.

35. Gören, A.; Mendes, J.; Rodrigues, H. M.; Sousa, R. E.; Oliveira, J.; Hilliou, L.; Costa, C. M.; Silva, M. M.; Lanceros-Méndez, S. High Performance Screen-Printed Electrodes Prepared by a Green Solvent Approach for Lithium-Ion Batteries. *Journal of Power Sources* **2016,** *334*, 65-77.

36. Ferreira, J. C. C.; Monteiro, T. S.; Lopes, A. C.; Costa, C. M.; Silva, M. M.; Machado, A. V.; Lanceros-Mendez, S. Variation of the Physicochemical and Morphological Characteristics of Solvent Casted Poly(Vinylidene Fluoride) Along Its Binary Phase Diagram with Dimethylformamide. *Journal of Non-Crystalline Solids* **2015,** *412*, 16-23.

37. Cabeza, O.; Varela, L. M.; Rilo, E.; Segade, L.; Domínguez-Pérez, M.; Ausín, D.; de Pedro, I.; Fernández, J. R.; González, J.; Vazquez-Tato, M. P.; Arosa, Y.; López-Lago, E.; de la Fuente, R.; Parajó, J. J.; Salgado, J.; Villanueva, M.; Matveev, V.; Ievlev, A.; Seijas, J. A. Synthesis, Microstructure and Volumetry of Novel Metal Thiocyanate Ionic Liquids with [Bmim] Cation. *Journal of Molecular Liquids* **2019,** *283*, 638-651.

38. Correia, D. M.; Costa, C. M.; Lizundia, E.; Sabater i Serra, R.; Gómez-Tejedor, J. A.; Biosca, L. T.; Meseguer-Dueñas, J. M.; Gomez Ribelles, J. L.; Lanceros-Méndez, S. Influence of Cation and Anion Type on the Formation of the Electroactive B-Phase and Thermal and Dynamic Mechanical Properties of Poly(Vinylidene Fluoride)/Ionic Liquids Blends. *The Journal of Physical Chemistry C* **2019,** *123*, 27917-27926.

39. Tamaño-Machiavello, M. N.; Costa, C. M.; Molina-Mateo, J.; Torregrosa-Cabanilles, C.; Meseguer-Dueñas, J. M.; Kalkura, S. N.; Lanceros-Méndez, S.; Sabater i Serra, R.; Gómez Ribelles, J. L. Phase Morphology and Crystallinity of Poly(Vinylidene Fluoride)/Poly(Ethylene Oxide) Piezoelectric Blend Membranes. *Materials Today Communications* **2015,** *4*, 214-221.

40. Correia, D. M.; Costa, C. M.; Rodríguez-Hernández, J. C.; Tort Ausina, I.; Biosca, L. T.; Torregrosa Cabanilles, C.; Meseguer-Dueñas, J. M.; Lanceros-Méndez, S.; Gomez Ribelles, J. L. Effect of Ionic Liquid Content on the Crystallization Kinetics and Morphology of Semicrystalline Poly(Vinylidene Fluoride)/Ionic Liquid Blends. *Crystal Growth & Design* **2020,** *20*, 4967-4979.

41. Correia, D. M.; Costa, C. M.; Nunes-Pereira, J.; Silva, M. M.; Botelho, G.; Ribelles, J. L. G.; Lanceros-Méndez, S. Physicochemical Properties of Poly(Vinylidene Fluoride-Trifluoroethylene)/Poly(Ethylene Oxide) Blend Membranes for Lithium Ion Battery Applications: Influence of Poly(Ethylene Oxide) Molecular Weight. *Solid State Ionics* **2014,** *268*, 54-67.

42. Botelho, G.; Lanceros-Mendez, S.; Gonçalves, A. M.; Sencadas, V.; Rocha, J. G. Relationship between Processing Conditions, Defects and Thermal Degradation of Poly(Vinylidene Fluoride) in the B-Phase. *Journal of Non-Crystalline Solids* **2008,** *354*, 72-78.

43. Correia, D. M.; Barbosa, J. C.; Costa, C. M.; Reis, P. M.; Esperança, J. M. S. S.; de Zea Bermudez, V.; Lanceros-Méndez, S. Ionic Liquid Cation Size-Dependent Electromechanical Response of Ionic Liquid/Poly(Vinylidene Fluoride)-Based Soft Actuators. *The Journal of Physical Chemistry C* **2019,** *123*, 12744-12752.

44. Costa, C. M.; Sencadas, V.; Pelicano, I.; Martins, F.; Rocha, J. G.; Lanceros-Mendez, S. Microscopic Origin of the High-Strain Mechanical Response of Poled and Non-Poled Poly(Vinylidene Fluoride) in the B-Phase. *Journal of Non-Crystalline Solids* **2008,** *354*, 3871-3876.

45. Park, M.; Zhang, X.; Chung, M.; Less, G. B.; Sastry, A. M. A Review of Conduction Phenomena in Li-Ion Batteries. *Journal of Power Sources* **2010,** *195*, 7904-7929.

46. Silva, M. M.; Barbosa, P. C.; Rodrigues, L. C.; Gonçalves, A.; Costa, C.; Fortunato, E. Gelatin in Electrochromic Devices. *Optical Materials* **2010,** *32*, 719-722.

47. Barbosa, J. C.; Correia, D. M.; Gonçalves, R.; de Zea Bermudez, V.; Silva, M. M.; Lanceros-Mendez, S.; Costa, C. M. Enhanced Ionic Conductivity in Poly(Vinylidene Fluoride) Electrospun Separator Membranes Blended with Different Ionic Liquids for Lithium Ion Batteries. *Journal of Colloid and Interface Science* **2021,** *582*, 376-386.

48. Wang, A.; Xu, H.; Liu, F.; Liu, X.; Wang, S.; Zhou, Q.; Chen, J.; Yang, S.; Zhang, L. Polyimide-Based Self-Standing Polymer Electrolyte Membrane for Lithium-Ion Batteries. *Energy Technology* **2018,** *6*, 326-332.

49. Fu, J.; Lu, Q.; Shang, D.; Chen, L.; Jiang, Y.; Xu, Y.; Yin, J.; Dong, X.; Deng, W.; Yuan, S. A Novel Room Temperature Poss Ionic Liquid-Based Solid Polymer Electrolyte. *Journal of Materials Science* **2018,** *53*, 8420-8435.

50. Shang, D.; Fu, J.; Lu, Q.; Chen, L.; Yin, J.; Dong, X.; Xu, Y.; Jia, R.; Yuan, S.; Chen, Y.; Deng, W. A Novel Polyhedral Oligomeric Silsesquioxane Based Ionic Liquids (Poss-Ils) Polymer Electrolytes for Lithium Ion Batteries. *Solid State Ionics* **2018,** *319*, 247-255.

51. Serra, J. P.; Pinto, R. S.; Barbosa, J. C.; Correia, D. M.; Gonçalves, R.; Silva, M. M.; Lanceros-Mendez, S.; Costa, C. M. Ionic Liquid Based Fluoropolymer Solid Electrolytes for Lithium-Ion Batteries. *Sustainable Materials and Technologies* **2020,** *25*, e00176.

52. Polu, A. R.; Rhee, H.-W. Ionic Liquid Doped Peo-Based Solid Polymer Electrolytes for Lithium-Ion Polymer Batteries. *International Journal of Hydrogen Energy* **2017,** *42*, 7212-7219.

53. Nien, Y.-H.; Carey, J. R.; Chen, J.-S. Physical and Electrochemical Properties of Lifepo4/C Composite Cathode Prepared from Various Polymer-Containing Precursors. *Journal of Power Sources* **2009,** *193*, 822-827.

54. Guo, J.; Sun, A.; Chen, X.; Wang, C.; Manivannan, A. Cyclability Study of Silicon–Carbon Composite Anodes for Lithium-Ion Batteries Using Electrochemical Impedance Spectroscopy. *Electrochimica Acta* **2011,** *56*, 3981-3987.

55. Costa, C. M.; Kundu, M.; Dias, J. C.; Nunes-Pereira, J.; Botelho, G.; Silva, M. M.; Lanceros-Méndez, S. Mesoporous Poly(Vinylidene Fluoride-Co-Trifluoroethylene) Membranes for Lithium-Ion Battery Separators. *Electrochimica Acta* **2019,** *301*, 97-106.

56. Chang, B.-Y.; Park, S.-M. Electrochemical Impedance Spectroscopy. *Annual Review of Analytical Chemistry* **2010,** *3*, 207-229.

57. Bao, J.; Qu, X.; Qi, G.; Huang, Q.; Wu, S.; Tao, C.; Gao, M.; Chen, C. Solid Electrolyte Based on Waterborne Polyurethane and Poly(Ethylene Oxide) Blend Polymer for All-Solid-State Lithium Ion Batteries. *Solid State Ionics* **2018,** *320,* 55-63.

58. Kimura, K.; Tominaga, Y. Understanding Electrochemical Stability and Lithium Ion-Dominant Transport in Concentrated Poly(Ethylene Carbonate) Electrolyte. *ChemElectroChem* **2018,** *5,* 4008-4014.

59. Li, X.; Wang, Z.; Lin, H.; Liu, Y.; Min, Y.; Pan, F. Composite Electrolytes of Pyrrolidone-Derivatives-Peo Enable to Enhance Performance of All Solid State Lithium-Ion Batteries. *Electrochimica Acta* **2019,** *293,* 25-29.

TOC graphic

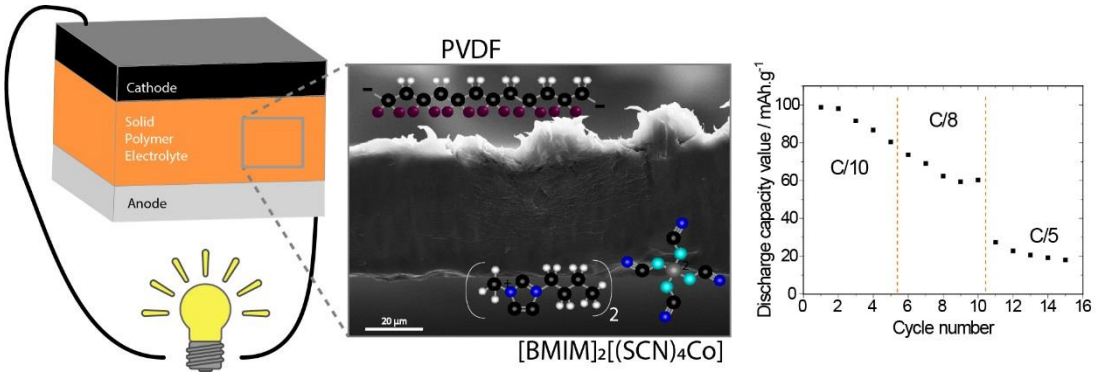
Cathode
Solid
Polymer
Electrolyte
Anode
PVDF
20 µm
[BMIM]2[(SCN)4Co]
Discharge capacity value / mAh.g-1
Cycle number
C/10
C/8
C/5